

Modeling of Storm Surges in the Bering Sea and Norton Sound

WALTER R. JOHNSON AND ZYGMUNT KOWALIK

Institute of Marine Science, University of Alaska, Fairbanks

Sea level, currents, and ice distribution are studied in the Bering Sea during storm events. The ice and ice edge are incorporated into storm surge model. The interaction of wind, ice, and water is expressed by the normal and tangential stresses. A numerical grid is established for the Bering Sea, and a second refined grid is constructed for Norton Sound. Construction of open boundary conditions for the water and ice motion and numerical questions related to the application of a large frictional coefficient for ice are also discussed. Storm events from February and March 1982 are analyzed and compared with observations of bottom pressure and ice motion made by NOAA Pacific Marine Environmental Laboratory in the Bering Sea and sea level observations at Stebbins, Alaska. The influence of the ice on the storm surge propagation is shown, particularly that of the fast ice in Norton Sound. The model reproduces several observed features of the ice distribution in the Bering Sea, including the "race track" region off Nome, the polynya south of Saint Lawrence Island, and the movement of the ice edge.

1. INTRODUCTION

The Bering Sea has one of the largest continental shelves in the world. Along this shelf, during late summer and fall, low-pressure systems generate storm surge waves. Two regions of the Bering Sea, Bristol Bay and Norton Sound, are obvious candidates for large sea level variations. Shallow Norton Sound, with an average depth of about 20 m, leads to strong amplification of the storm wave, especially in conjunction with west and southwest winds.

The knowledge of sea level changes caused by storm surges in Norton Sound is quite modest owing primarily to the absence of any permanent tide gauges in this area. The frequency of major storms, when compared with that in the other regions of the Bering Sea, is rather low. Late summer and fall storms, if they generate south, southwest, or northwest winds, can cause extensive flooding to the coastal areas of low relief surrounding Norton Sound. The main storm track during summer and fall is toward the north and northeast [Brower *et al.*, 1977]. Storm surges of as much as 4 m have occurred in this area, and the most recent storm of such intensity was in November 1974 [Fathauer, 1978]. The most severe flooding occurred at Nome, Alaska, where the damage sustained was estimated at \$12 million. The low-pressure system moved from the Aleutians to the Bering Sea. Winds as high as 39 m/s were recorded. The extent of flooding was tracked by the U.S. Geological Survey through an observation of the driftwood and debris line after the storm [Sallenger, 1983]. This storm has been used as the wind forcing for one of the model cases (section 4.3). Surges of 1 to 2 m regularly flood the Norton Sound area and cause serious problems to the coastal communities [Wise *et al.*, 1981]. Until recently, tide gauges were installed in this region only for short periods of time. Sea level data were recorded in Norton Sound during a sediment transport study in summer and fall 1977 [Cacchione and Drake, 1979].

In 1978 a set of sea level data was gathered over the shelf by Schumacher and Tripp [1979]. An extensive observational study of tides and tidal currents in the northeastern Bering Sea from November 1981 until August 1982 was conducted by NOAA Pacific Marine Environmental Laboratory (PMEL) [Moffeld, 1984]. At the same time, sea level was recorded at a

nearshore station in Stebbins, Alaska (R. Mitchel, personal communication, 1983), an area where fast ice usually occurs in winter. During 1982, ice drift motion was also studied from several Argos drifting ice platforms [Reynolds and Pease, 1984]. This set of diverse data gave a good opportunity to test our model, especially the influence of nearshore fast ice on the storm surge wave propagation.

Wise *et al.* [1981] compiled all available data on the storm surges and were able to identify 13 floodings at Nome and 10 at Unalakleet, Alaska. Although the present set of data is too small to estimate a statistically valid distribution of the sea level variations, these statistics may serve as a first approach to the prediction of the surge range.

The lack of knowledge on the sea level distribution can be ameliorated by applying numerical modeling. Leendertse and Liu [1981] developed a three-dimensional model of Norton Sound to study the density and tide-driven motion. We have applied a model to study storm surge in the Norton Sound area based on a model previously tested in the Beaufort and Chukchi Seas [Kowalik and Matthews, 1982; Kowalik, 1984]. To drive the storm surge model, suitable wind data are required; we used the surface pressure charts to compute the geostrophic and surface winds. First, geostrophic wind was computed from the atmospheric pressure, then the "true" wind was computed by application of empirical coefficients [Albright, 1980; Walter and Overland, 1984]. The winds were computed over larger scales than the model grids. Any effects of artificially introduced wind stress curl are small in the model ocean currents, since the currents are depth averaged and divergences result in small sea level variations. Stress curl variations could introduce some undesired variations in the ice compactness field, but they were not significant.

In the polar regions, ice cover modifies the transfer of momentum from the atmosphere to the ocean, thus influencing the spatial and temporal distribution of the storm surges [Henry, 1974]. Therefore together with a storm surge model for the Beaufort and Chukchi Seas, a scheme to include ice cover was developed. In the present study we apply the linear frictional law not only for the pack ice but for the shorefast ice as well. The fast ice is distributed in the nearshore zone of Norton Sound. The results from the model computation are compared with the sea level measurements taken under the fast ice at Stebbins in February and March 1982. Various constitutive laws to describe sea ice, proposed by Coon *et al.* [1974] and Hibler [1979], contain both mechanical and thermal properties of ice. Since storm surge is a phenomenon of

Copyright 1986 by the American Geophysical Union.

Paper number 6C0039.
0148-0227/86/006C-0039\$05.00

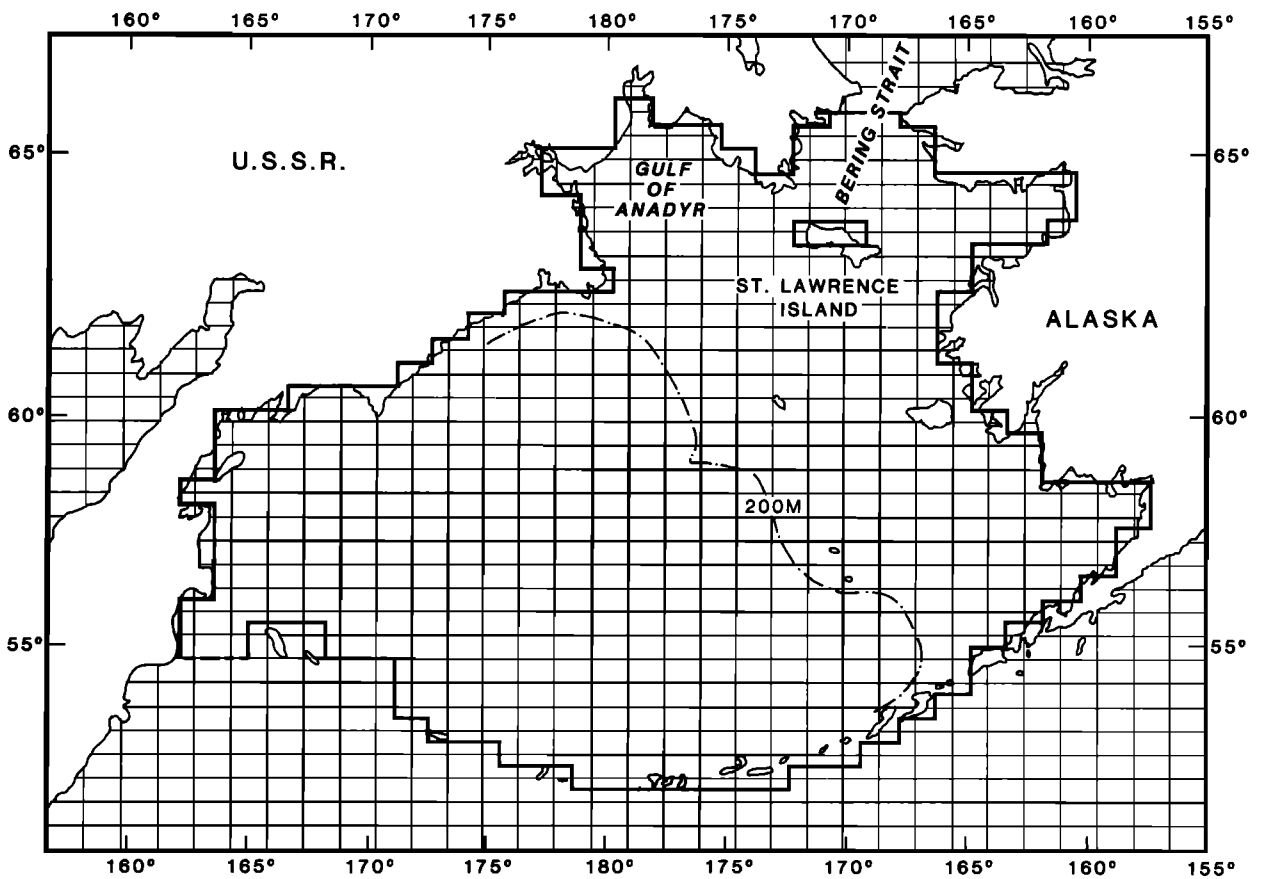
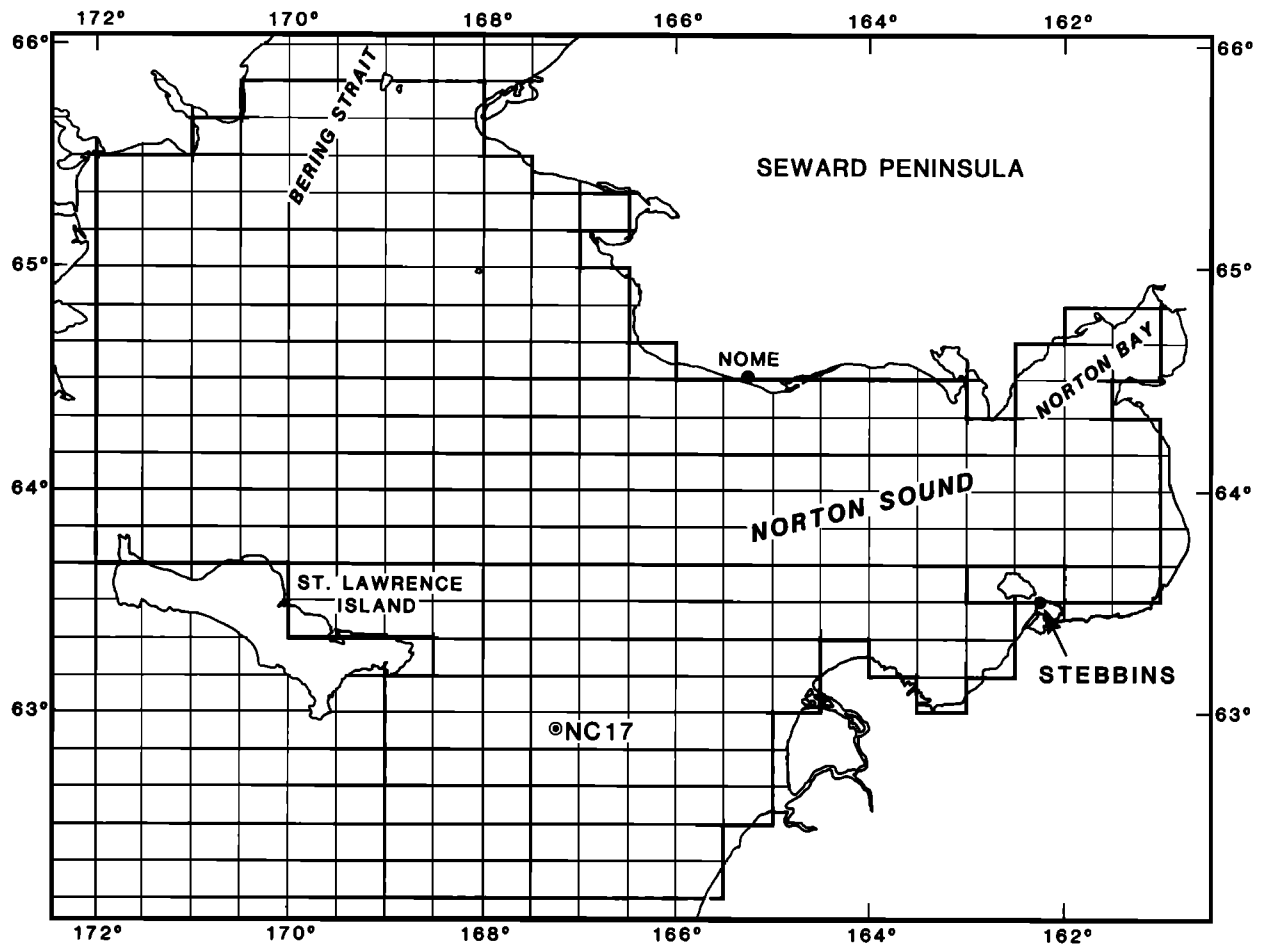


Fig. 1. Chart showing model regions. The upper panel is the grid used for the detailed Norton Sound model. The upper panel also shows the locations of the comparison points Stebbins, Alaska, and station NC17 and the location of Nome, Alaska. The lower panel is the grid used for the Bering Sea model. Broken lines indicate open (sea) boundaries.

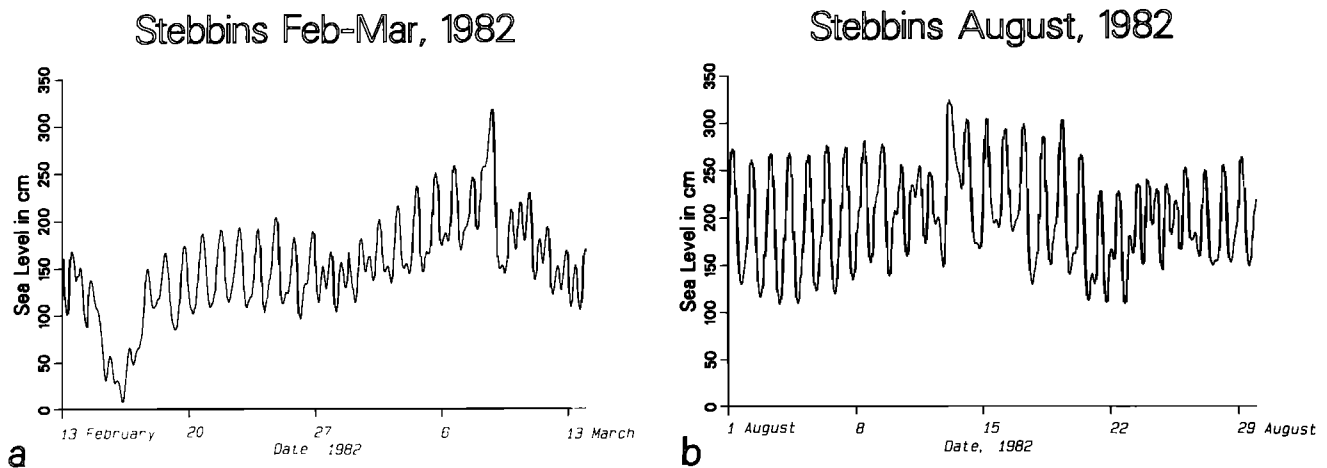


Fig. 2. (a) Time series of sea level measurements from Stebbins, Alaska, February and March 1982. Notice two surges: February 14–18 and March 7–9. (b) Time series of sea level measurements from Stebbins, Alaska, August 1982.

short duration, the thermal properties of ice growth and decay can be neglected, and only ice mechanics needs to be considered. Hence a simpler constitutive law has been implemented, as was proposed by *Doronin* [1970]. Ice motion in Norton Sound has been studied by *Stringer and Hensler* [1981]. Direct comparison of the ice motion observed through the satellite imagery with the ice movement computed by the model seems to be the best approach to validate this aspect of the model. Unfortunately, the acquisition of the cloud-free images during storms has a rather small probability.

Air-ice interaction has been studied both from ice floe stations and from aircraft. *Macklin* [1983] reported a wind drag coefficient over ice of 3.1×10^{-3} . Measurements by *Walter and Overland* [1984] gave a similar value for the drag coefficient. These values are among the largest for the polar seas [*Leavitt*, 1980].

The steady state slab models of the wind-driven ice drift developed for the Bering Sea Shelf by *Pease and Overland* [1984] and *Overland et al.* [1984] show a very good correlation with the observed ice motion. Through the application of these models it has been established that the influence of the bathymetry on the wind drift of ice in shallow seas is constrained to water depth of less than 30 m.

Storm surges occur together with astronomical tides, and therefore it is essential to understand the tide distribution. An approximate tide distribution in Norton Sound is known through observations and numerical modeling [*Pearson et al.*, 1981; *Moffeld*, 1984]. A tidal range of the order of 1 m to 1.5 m can be expected. The semidiurnal (M_2) component has an amphidromic point in Norton Sound; therefore the diurnal components dominate the tidal regime.

2. NUMERICAL MODELING: AREA, GRID, AND BOUNDARY CONDITIONS

The bases of the calculations are the vertically integrated equations of water motion and continuity and the equations of ice motion and conservation described by *Kowalik* [1984]. The interaction of the atmosphere, ice, and water is expressed in these equations by the stresses. The internal ice stresses are given by the linear frictional model.

The approach has been tested for the Beaufort and Chukchi Seas under pack ice conditions. Here we would like to apply the same set of equations to a new region and also to include a nearshore fast ice. The fast ice mechanics is expressed by a linear frictional formula with large viscosity coefficients.

The main modeling effort is confined to Norton Sound (Figure 1). The Norton Sound model has three open boundaries (broken lines); in the Bering Strait, between Siberia and Saint Lawrence Island, and between Saint Lawrence Island and Alaska. The grid intervals of the numerical lattice are $\frac{1}{2}$ of a degree of latitude and 0.5° of longitude. To check the validity of the model with the open boundaries we also compute the storm surges throughout the Bering Sea area with a larger numerical grid spacing of 0.5° of latitude and 1.5° of longitude (Figure 1). The application of the radiation condition by *Reid and Bodine* [1968] and the modified versions by *Camerlengo and O'Brien* [1980] and *Raymond and Kuo* [1984] lead to a distorted sea level distribution in the Norton Sound model. Such behavior of the solution may be related to the depth distribution, since the average depth of Norton Sound is about 20 m and the open boundaries of the numerical model were located at the 30- to 50-m depth.

Normally, in a storm surge computation the radiating boundary is situated beyond the shelf break (and/or far away from the region of interest), and the comparison of calculated and measured sea level in the shelf zone is quite satisfactory. The radiation condition is applied to waves generated inside the domain of integration. In those instances when only certain portions of the shelf are considered, waves generated outside the domain may influence the solution. Therefore to solve the equations of water motion and continuity in Norton Sound, first the solution for the entire Bering Sea is sought. Then the distribution of velocity and sea level at the open boundary of the refined model is defined by linear interpolation from the results of those calculations.

The boundary conditions for the ice motion are neither understood nor readily available. For the equations of ice motion we found that the best results are derived by assuming a continuity of velocity along the normal to the open boundary.

In the first series of experiments, the equation of ice transport (Equation (6) of *Kowalik* [1984]) was solved with known compactness along the open boundaries. An ice distribution closer to the observed one has been obtained by applying an advection equation,

$$\frac{\partial c}{\partial t} + v \frac{\partial c}{\partial x} = 0 \quad (1)$$

along the direction (x) normal to the open boundary. Details of the numerical implementation are given in the appendix.

TABLE 1. Amplitude and Phase of the Principal Tidal Constituents at Stebbins, Alaska

Constituent	Frequency, cpd	Summer		Winter		
		Amplitude H_s , cm	Phase G_s , deg	Amplitude H_w , cm	Phase G_w , deg	H_w/H_s
Q_1	0.89324	5.01	34.8	2.91	359.4	0.58
O_1	0.92954	25.81	61.9	14.98	30.1	0.58
M_1	0.96645	1.83	89.1	1.06	61.0	0.58
P_1	0.99726	15.69	112.2	10.28	87.3	0.65
K_1	1.00274	47.41	116.3	31.07	91.9	0.65
J_1	1.03903	2.04	143.3	1.18	122.6	0.58
$2N_2$	1.85969	0.96	109.6	0.92	27.0	0.96
μ_2	1.86455	1.15	117.7	1.11	35.7	0.96
N_2	1.89598	7.21	170.3	6.91	91.3	0.96
v_2	1.90084	1.40	178.5	1.34	100.0	0.96
M_2	1.93227	19.46	231.1	13.40	155.6	0.69
L_2	1.96857	0.54	288.4	0.38	176.8	0.70
T_2	1.99726	0.28	333.7	0.10	193.6	0.36
S_2	2.00000	4.70	338.0	1.76	195.2	0.37
K_2	2.00548	1.28	346.6	0.48	198.4	0.37

3. INFLUENCE OF ICE ON LONG WAVE PROPAGATION: MEASUREMENT AND MODELING

We are not able to measure the same storm surge in the summer and winter, but this is possible for the astronomical tide wave. The sea level recorded under the fast ice at Stebbins in February–March 1982 (Figure 2a) and in August 1982 (Figure 2b) displays a clear difference in the tide amplitude. The harmonic analysis (Table 1) shows that the amplitudes H of the main constituents, K_1 , O_1 , and M_2 , increase from winter (H_w) to summer (H_s) by about 40%. We therefore expect an inhibitory effect on the storm surge by fast ice as well. In addition, fast ice may produce a shift in the time of arrival of the surge wave.

The influence of fast ice on the storm wave is studied through a linear viscous model of the ice internal stress.

Internal ice stresses F_i in the equations of motion are expressed by a linear viscous model

$$F_i = \eta \frac{\partial^2 v_i}{\partial x_j \partial x_j} \quad (2)$$

with the magnitude of kinematic viscosity coefficient (η) ranging from 5×10^8 cm²/s to 5×10^{12} cm²/s. In (2), v_i are the east (v_1) and north (v_2) components of the ice velocity.

Numerical solutions of the storm surge problems are usually obtained by applying an explicit in time and staggered in space numerical scheme proposed by Hansen [1962]. For a large viscosity coefficient the explicit scheme is unstable [Kowalik, 1981]. Therefore to model fast ice (which is parameterized by a large value of viscosity coefficient), a modified scheme of numerical computation, unconditionally stable in time, has been introduced (see appendix). The difference between the pack ice and fast ice will be expressed through the different values of the viscosity coefficient η .

To define the ice friction coefficient suitable for the storm surge propagation in the fast ice, the magnitude of the coefficient which will cause the ice velocity to be nearly zero must be determined. For this purpose a series of numerical experiments was carried out with the whole area of Norton Sound covered by fast ice ($c = 1$) and applying a friction coefficient from the range 1 cm²/s to 5×10^{12} cm²/s. Friction through the viscous stresses suppresses the ice motion, and when the ice friction coefficient attains 10^{12} cm²/s, the ice velocity is close to zero (Figure 3). Because water motion depends on the

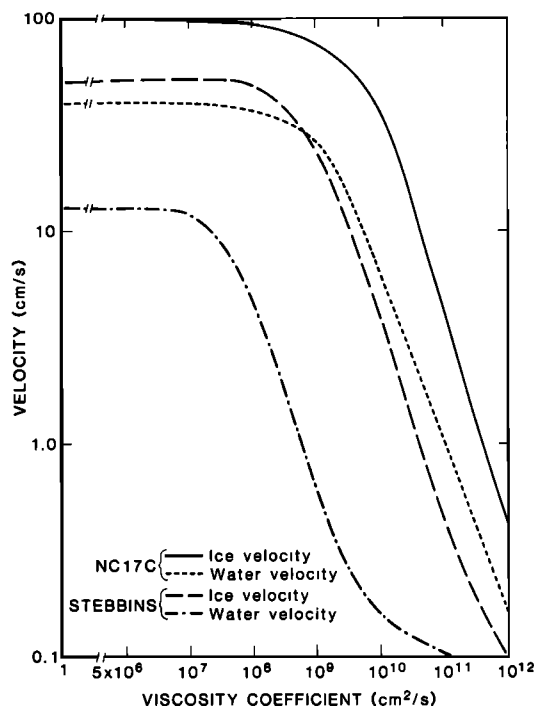


Fig. 3. Water and ice velocity as a function of the viscosity coefficient of the ice at two locations in Norton Sound. The domain is covered by ice with 0.99 compactness.

energy transfer from the atmosphere to the water through the ice cover, the high values of ice friction coefficient and ice compactness $c = 0.99$ lead to suppression of the water motion as well. The motion decreased more at the nearshore location (Stebbins) than in the open sea region (NC17) probably because of the higher bottom friction. In the real cases, fast ice never covered the whole Norton Sound area but covered only a narrow nearshore band; therefore the damping of the surge wave under the pack ice was only partial.

The choice of the friction coefficient for the pack ice modeling is a more complicated problem. To test the model against measurements, we have simulated two storm surges from February 12–19 and March 7–11, 1982 (see Figure 2a). During this period, NOAA deployed ice-drifting stations. Through a comparison of the ice drift motion of the NOAA stations set on the pack ice and the drift computed by the

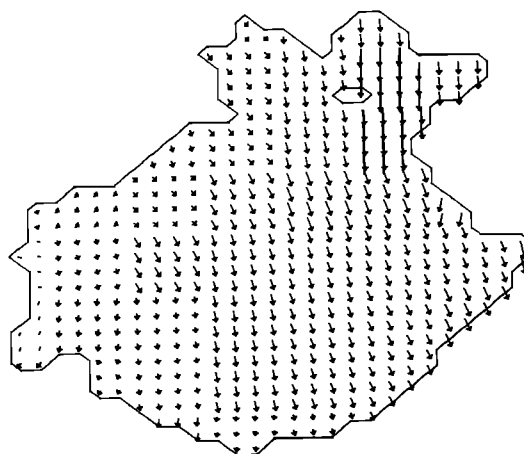


Fig. 4. Surface wind distribution over the Bering Sea for 0000 UT February 17, 1982. One vertical grid distance is scaled to 10 m/s.

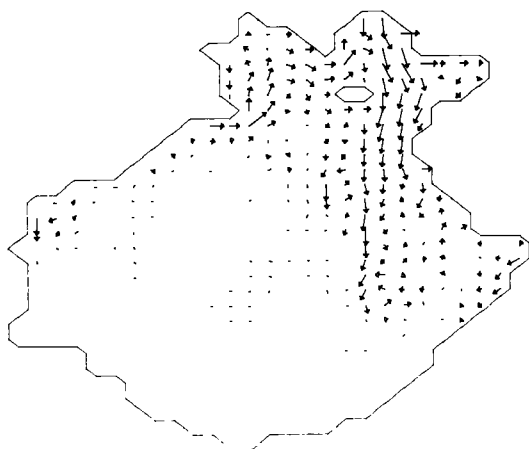


Fig. 5. Vertically averaged velocity in the Bering Sea for 0000 UT February 17, 1982. One vertical grid distance is scaled to 20 cm/s.

model, we found that for a compactness of 0.7 to 0.8 the viscosity coefficient η ranged from 5×10^8 cm²/s to 5×10^9 cm²/s [Kowalik and Johnson, 1985].

4. STORM SURGES IN THE BERING SEA AND NORTON SOUND

The late summer storms are often caused by the low-pressure centers which in the northeastern Bering Sea generate positive sea level changes. During the winter the weather over the Bering Sea depends on the east Siberian high-pressure system. The northeasterly winds generate negative sea levels in the Norton Sound area and the ice movement from the northeastern Bering Sea toward the south [Muench and Ahlnäs, 1976]. Norton Sound is situated in the northeastern region of the Bering Sea as a relatively shallow embayment of about 200 km in length. Large portions of Norton Sound have a depth of less than 10 m, and the average depth is about 20 m [Muench et al., 1981]. During the storm-dominated season from August to November, an average of two to four low-pressure systems with wind velocity ranging from 15 to 25 m/s may hit the Norton Sound area. The Norton Sound shore is generally of low relief, and during storms the coastal plains can be inundated by the surge of wind waves superimposed on the surge wave.

To test the model against measurements, we have simulated two storms which occurred in 1982. The first storm was driven by a high-pressure system with the center situated over eastern Siberia during February 12–19, 1982, which caused a negative

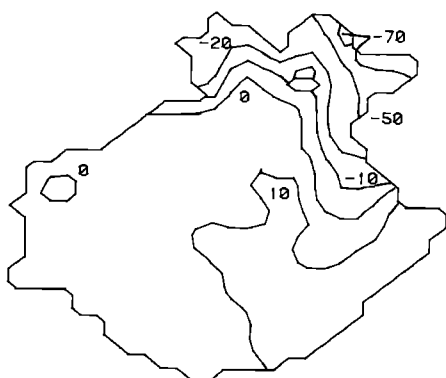


Fig. 6. Sea level distribution in the Bering Sea for 0000 UT February 17, 1982. Numbers are given in centimeters.

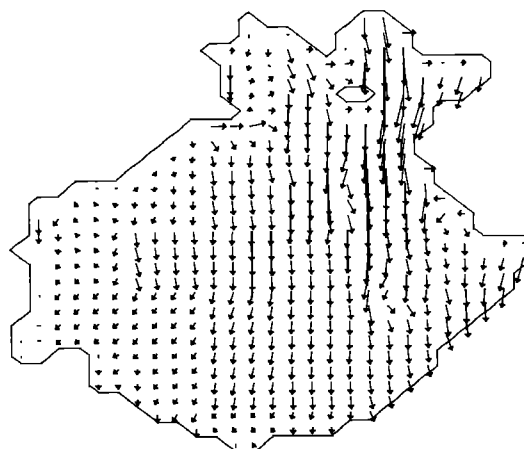


Fig. 7. Ice velocity distribution in the Bering Sea for 0000 UT February 17, 1982. One vertical grid distance is scaled to 20 cm/s.

surge in the Norton Sound area. The second storm occurred from March 7 to 11, 1982, with a low-pressure center traveling from the central Bering Sea towards the northeastern Bering Sea. The southwesterly winds generated a positive surge of about 1 to 2 m in Norton Sound. The ice distributions we used for the simulations were from the charts prepared by the Navy-NOAA Joint Ice Center, Naval Polar Oceanography Center, recalculated as compactness. We have used two measuring stations where the sea level was recorded during the storm surge passage. At one point, located at $\phi = 62^{\circ}53'N$, $\lambda = 167^{\circ}04'W$, a bottom pressure gauge (designated NC17) was situated under the pack ice [Moffeld, 1984]. The second point was located close to Stebbins, Alaska ($\phi = 63^{\circ}30'N$, $\lambda = 162^{\circ}20'W$), and the measurements were taken under the fast ice (J. Oswald, personal communication, 1983). The measurements in Stebbins should provide an ample opportunity to study the influence of fast ice on propagation of the long wave.

4.1. Storm Surge of February 1982

The meteorological observations at the time of the storm are described by Reynolds and Pease [1984]. The storm surge of February 12–19 was induced by the high-pressure system with the center located over eastern Siberia. Northeasterly winds up to 15 m/s caused a negative surge over the northeastern shelf and a positive level at the southeast end of the

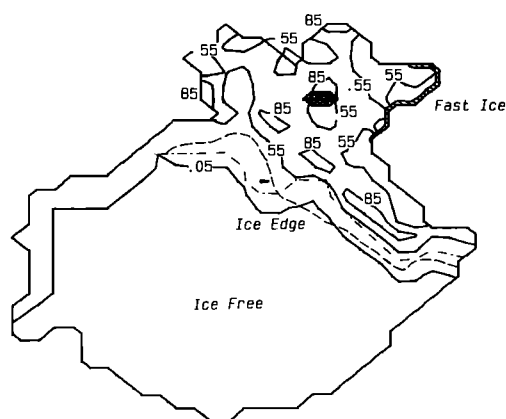


Fig. 8. Ice compactness distribution in the Bering Sea for 0000 UT February 17, 1982. The dashed/dotted line shows the initial position of the observed ice edge. The dashed line shows the observed position of the ice edge on February 16, 1982.

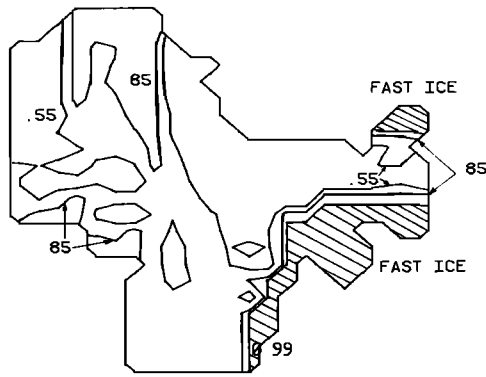


Fig. 9. Ice compactness distribution in the northeastern Bering Sea for 0000 UT February 17, 1982.

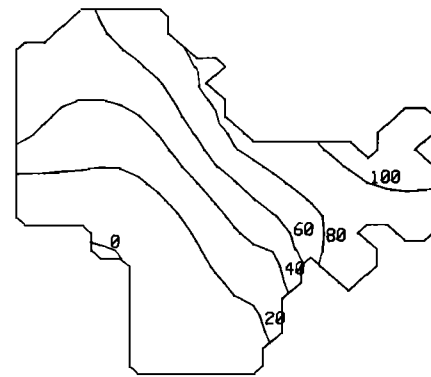


Fig. 11. Sea level distribution in the northeastern Bering Sea for 0600 UT March 9, 1982. Numbers are given in centimeters.

Bering Sea. The numerical model reproduces a 7-day period from 0000 UT February 12 to 0000 UT February 19. The surface wind used to drive the model was calculated over the entire Bering Sea every 6 hours from the surface pressure maps. The wind was linearly interpolated for the shorter time steps of the numerical computations. The wind chart for 0000 UT February 17 is plotted in Figure 4. The wind directions during the computation were fairly steady. Quasi-steady north-northeast winds generated a wind-driven current mainly along the Bering Shelf (Figure 5). About 2–3 days after the beginning of the storm a southward and southwestward flow along the eastern part of the shelf is compensated for by northward and northeastward flow in Anadyr Bay and Anadyr Strait. Currents in Anadyr Bay flow in the opposite direction to the wind; therefore such flow is due to the sea level distribution (Figure 6).

The southward and southwestward flow along the eastern Bering Shelf follows the bottom and coastal contours. In the shallow embayments like Norton Sound, the flow is directed to the east along the northern shore and to the west along the southern shore. Two regions of different dynamics can be singled out from Figure 5: the high-velocity area extended from the Bering Strait to the straits between Saint Lawrence Island and the Alaskan coast, and an area of small and variable velocities in Norton Sound.

Since the wind for this case was strongly from the north-northeast, a lowering of sea level along the northeastern shelf occurred (Figure 6). The sea level contours and current direc-

tion tend to be parallel (Figures 5 and 6), as may be expected in a depth-averaged model. The maximum change occurred on February 16 and 17, when the level dropped to -1 m in Norton Sound. Ice velocity as high as 0.6 m/s occurred over the shelf (Figure 7). The north and northeast winds pushed the ice from north to south with especially high velocity between Saint Lawrence Island and Norton Sound, the area which is known from satellite and aircraft observation as a “race track” [Ray and Dupré, 1981]. The ice motion is much more strongly coupled than the water motion to the wind magnitude and direction.

Ice concentration (or ice compactness) is plotted at the maximum of sea level change (Figure 8). Comparison of the observed and computed ice edge location after the storm shows that the model is able to predict the correct direction of the ice edge motion over much of the domain.

By applying a high-resolution local model of the Norton Sound area (Figure 1, upper panel), the detailed picture of the flow and ice distribution can be studied. As an example a distribution of the ice compactness for February 17, 1982, is depicted in Figure 9. Except for the southern nearshore region of Norton Sound and the Norton Bay area where fast ice ($c = 0.99$) was set as a permanent feature, the initial ice compactness in Norton Sound was set constant everywhere ($c = 0.7$), and at the northern boundary (Bering Strait) the compactness was assumed to be constant and equal to 0.9. The northeasterly wind sets a dominant ice pattern with areas

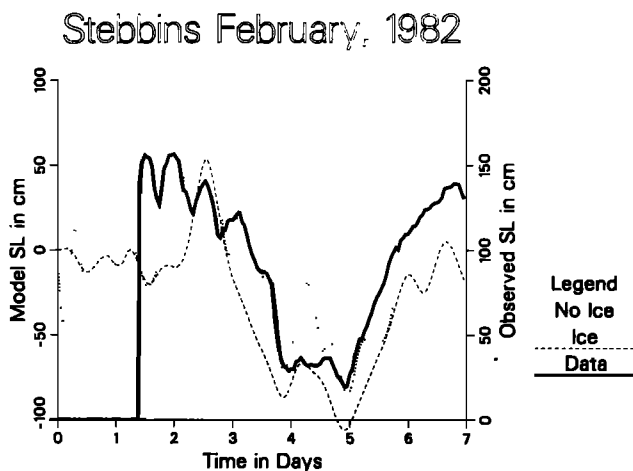


Fig. 10. Model comparison with observed sea level at Stebbins, Alaska.

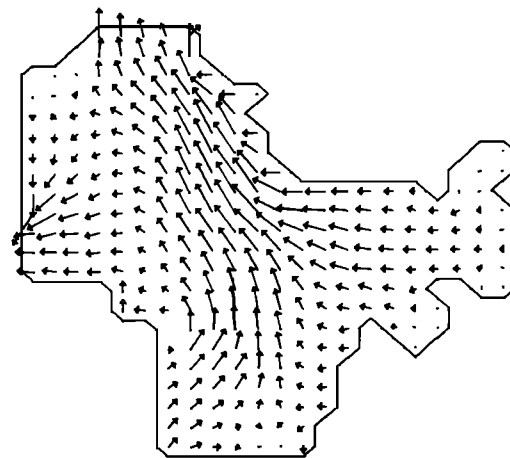


Fig. 12. Vertically averaged velocity in the northeastern Bering Sea for 0600 UT March 9, 1982. One vertical grid distance is scaled to 20 cm/s.

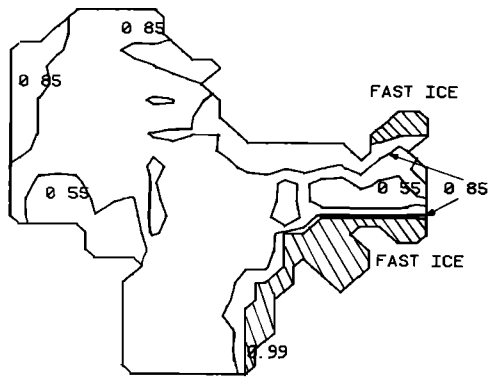


Fig. 13. Ice compactness distribution in the northeastern Bering Sea for 0600 UT March 9, 1982.

of low compactness along the northern shore of Norton Sound and a band of high compactness ($c = 0.85$) southward from the Bering Strait. The influence of Saint Lawrence Island on the ice distribution is also eminent; at the windward side of the island a high compactness was produced, a feature corroborated by observations [McNutt, 1981]. Resultant ice distribution is closely related to the ice velocity. A change in the ice motion between Norton Sound and the Bering Sea noticed by Stringer and Henzler [1981] is also apparent in our computations (Figure 7).

Three time series of sea level during the February storm surge in Stebbins are plotted in Figure 10. Observed changes are given by a solid line, the level computed by the storm surge model without ice cover is shown by a dotted line, and the computed level with pack and fast ice is shown by a dashed line. The Stebbins observations were located under the fast ice; therefore the calculated sea level with fast ice shows essential differences from the ice-free computations.

4.2. Storm Surge of March 1982

Although the dominant wind pattern over the Bering Sea is related to a high-pressure system, the northwesterly wind is often reversed by low-pressure systems. A storm surge due to a low-pressure system occurred on March 8 and 9, 1982; the model computation spans the period 1800 UT March 7 to 1800 UT March 10.

The low-pressure system was composed of two or three low pressure centers which were situated over the central and east-

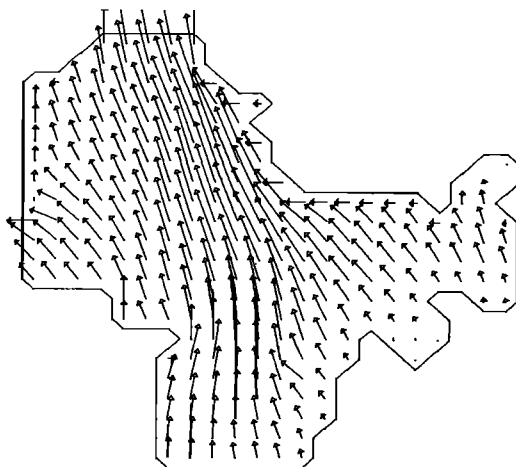


Fig. 14. Ice velocity distribution in the northeastern Bering Sea for 0600 UT March 9, 1982. One vertical grid distance is scaled to 20 cm/s.

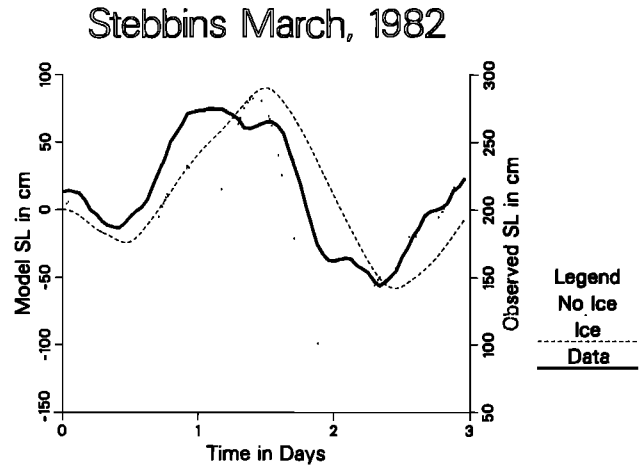


Fig. 15. Model comparison with observed sea level at Stebbins, Alaska.

ern Bering Sea. The low-pressure system displayed a slow movement toward the northeast; therefore during the first part of the storm, southwesterly winds generated a positive surge in Norton Sound. Later, when the low-pressure center was located over Alaska, the northwesterly winds caused a negative surge (Figure 2a) in Norton Sound. Storm-related changes of velocity and sea level are located along shallow northern and eastern regions of the Bering Sea. Although high ice velocity was observed, the ice distribution after the 3 days of the storm remained close to the initial distribution because the winds reversed. Based on the fine-grid model, the ice and water parameters are shown at the time of the highest sea level occurrence, about 36 hours from onset of storm, i.e., at 0600 UT March 9. The sea level increases from zero at Saint Lawrence Island to above 1 m in Norton Bay (Figure 11). The water motion indicates that the velocity is parallel to the sea level isolines (Figure 12).

The initial ice distribution is similar to case 1; thus except for the southern shore of Norton Sound and the Norton Bay area where the fast ice is located, the ice compactness over the Norton Sound region is constant and set at 0.7. Along the northern and northeastern shores the southwesterly wind produced an area of high compactness ($c = 0.85$). Close to Saint Lawrence Island the ice compactness has decreased to $c = 0.55$ (Figure 13). The regions of the fast ice stayed uniform during the entire computation, since the ice velocity was negligible in these regions. The ice velocity pattern (Figure 14)

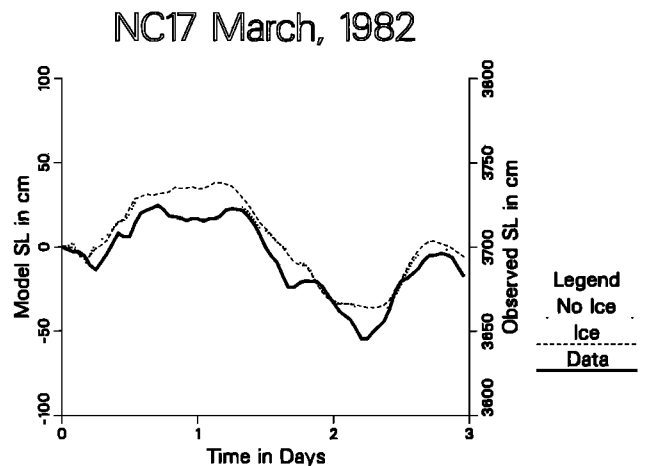


Fig. 16. Model comparison with observed sea level at point NC17.

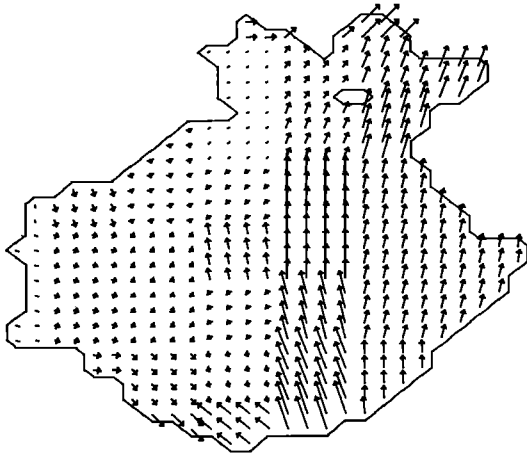


Fig. 17. Surface wind distribution over the Bering Sea for 0000 UT November 13, 1974. One vertical grid distance is scaled to 10 m/s.

follows the wind distribution. Again, owing to the flow constraints, the high-velocity region is generated between Saint Lawrence Island and Alaska. In this case, ice is transported into the Chukchi Sea.

To study the influence of ice cover on the storm surge propagation, the computations were performed with ice cover and with an ice-free sea surface. The results of the computations along with the recorded sea level in Stebbins and at station NC17 are plotted in Figures 15 and 16. The sea level changes at NC17 during the storm surge were calculated with the pack ice cover only, far from the fast ice zone, and they do not show large differences from the ice-free computations (Figure 16).

4.3. Storm Surge of November 1974

This storm surge was caused by a low-pressure system traveling from the Aleutian Islands to the Bering Strait. Winds of 25 m/s to 35 m/s were recorded [Fathauer, 1978]. Along the shores of Norton Sound, combined storm surge and wind waves reached as high as 5 m [Sallenger, 1983]. On November 11, 12, and 13, coastal communities from Bristol Bay to Kotzebue Sound were severely flooded and damaged. After the storm, observations of a debris line along the Norton Sound shore by Sallenger [1983] showed that at all but a few locations only one debris line was found. This would indicate that the storm surge of November 1974 was the strongest in recent history, since it had incorporated older debris lines. The numerical calculation spans the period from 0000 UT November 10 to 0000 UT November 14. The largest flooding indicated by the model calculation occurred between day 2 and day 3

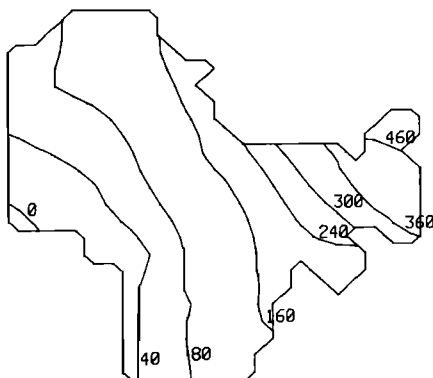


Fig. 18. Sea level distribution in the northeastern Bering Sea for 0000 UT November 13, 1974. Numbers are given in centimeters.

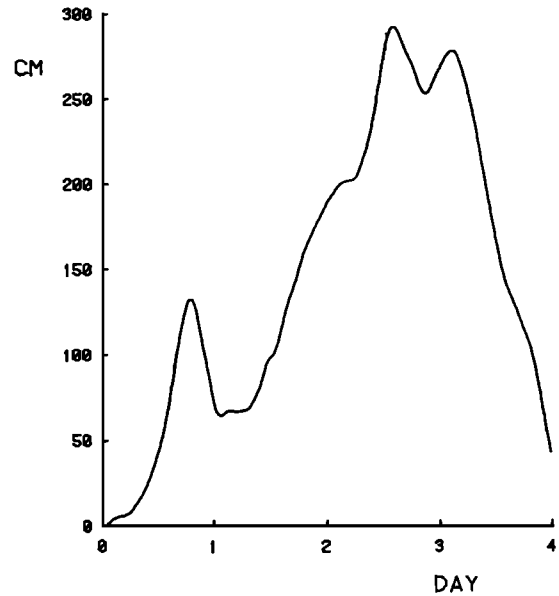


Fig. 19. Computed sea level time series at Nome from 0000 UT November 10 to 0000 UT November 14, 1974.

from the onset of computations, i.e., between November 12 and 13. To describe the weather pattern during the storm, the chart of wind distribution calculated from the surface pressure is given in Figure 17. South and southwesterly winds in the range 15 to 30 m/s generated a conspicuous surge (Figure 18). The surge wave did not interact with ice cover because apart from fresh ice in Norton Sound, the entire Bering Sea was ice-free. The results show that shallow water bodies such as Norton Sound enhance the surge wave. At the peak of the storm the sea level reached about 5 m in Norton Bay (Figure 18). Temporal variations of the sea level calculated for several locations along the shore show that the Norton Sound coast was severely flooded, with sea level higher than 2.5 m. In certain locations, like Nome, flooding occurred several times (Figure 19). Although no tide gauge observations are available to compare against computation, the magnitude of surge derived from the model compares well with debris line observations [Sallenger, 1983] and flood reports from Nome [Wise *et al.*, 1981].

5. CONCLUSIONS

Results from the storm surge computations show the relationships of the sea level and currents. In addition, the inclusion of fast ice in the model can produce some measurable differences in the results. The Bering Sea model reproduces several observed features of the ice distribution as well as predicts the sea level changes. The polynya south of Saint Lawrence Island, the movement of the ice edge, and the movement of the ice in the "race track" region are good examples. The Bering model is adequate to determine the boundary conditions for the Norton Sound region model. The Norton Sound model required the specification of velocity and sea level at the open boundaries. When the model was run with only radiation conditions on those boundaries, it did not reproduce the observed variations in sea level, because of the lack of interaction with the larger domain. The fact that the regional Norton Sound model had the boundaries in relatively shallow water appears to be the source of this difficulty. If the radiation boundary conditions can be applied in deep water, the model is less sensitive to the alongshore regions. With the boundaries specified by the Bering model, the Norton Sound

model made possible a more detailed examination of the surge within the sound, particularly in the regions of small-scale bathymetry near Stebbins and in Norton Bay.

APPENDIX: NUMERICAL FORMULATIONS

The difference between the pack ice and fast ice is expressed through the different values of the viscosity coefficient η . For a large viscosity coefficient the explicit numerical scheme is unstable [Kowalik, 1981]. Therefore to model fast ice (which is parameterized by a large value of viscosity coefficient), a modified scheme of numerical computation, unconditionally stable in time, has been introduced. We shall explain the approach only for one component of equation (2). The time variations of the E-W component of ice velocity caused by internal stresses are expressed by

$$\frac{\partial v}{\partial t} = \eta \left(\frac{\partial^2 v}{\partial x_1^2} + \frac{\partial^2 v}{\partial x_2^2} \right) \quad (\text{A1})$$

where v_1 is changed to v .

To integrate numerically the above equation, the time step T and space lattice with step h is introduced. Independent variables t , x_1 , and x_2 are expressed as $t = KT$, $x_1 = Lh$, $x_2 = Mh$, and the numerical form of (A1)

$$\begin{aligned} & \frac{v_{L,M}^{K+1} - v_{L,M}^K}{T} \\ &= \frac{\eta}{h} \left(\frac{v_{L+1,M}^K - v_{L,M}^K}{h} - \frac{v_{L,M}^{K+1} - v_{L-1,M}^{K+1}}{h} \right) \\ &+ \frac{\eta}{h} \left(\frac{v_{L,M+1}^K - v_{L,M}^K}{h} - \frac{v_{L,M}^{K+1} - v_{L,M-1}^{K+1}}{h} \right) \end{aligned} \quad (\text{A2})$$

is advancing solution in time from $t = KT$ to $t = (K+1)T$. This numerical scheme is unconditionally stable for any (positive) η . The actual computation is explicit, although the values $v_{L-1,M}^{K+1}$ and $v_{L,M-1}^{K+1}$ seem to be unknown. The computation takes place along increasing values of indices L and M ; thus when the solution is sought at the point (L, M) , the new values of variable v are already known at the points $(L, M-1)$ and $(L-1, M)$.

To advance the solution in time, the following explicit formula is used:

$$\begin{aligned} v_{L,M}^{K+1} = & \left\{ \frac{\eta T}{h^2} [v_{L+1,M}^K + v_{L-1,M}^{K+1} + v_{L,M+1}^K \right. \\ & \left. + v_{L,M-1}^{K+1} - 2v_{L,M}^K] + v_{L,M}^K \right\} / \left(1 + \frac{2\eta T}{h^2} \right) \end{aligned} \quad (\text{A3})$$

The method presented above is closely related to the angle derivative method [Roache, 1972].

The advection of ice into and out of the model domain is specified by boundary condition (1). Assuming the point at the boundary has coordinates L, M , the numerical form for (1)

$$\begin{aligned} & \frac{C_{L,M}^{K+1} - C_{L,M}^K}{T} + \frac{(v + |v|)}{2} \left(\frac{C_{L,M}^K - C_{L-1,M}^K}{h} \right) \\ & + \frac{(v - |v|)}{2} \left(\frac{C_0^K - C_{L,M}^K}{h} \right) = 0 \end{aligned} \quad (\text{A4})$$

will set compactness at the boundary as a function of velocity direction. Positive v is directed out of the integration domain. C_0^K is the ice compactness outside of the domain boundary and is assumed to be known from observation. It is advected into the domain by (A4) if the velocity across the boundary has a negative sign.

Acknowledgments. This study was funded wholly by the Mineral Management Service through interagency agreement with the National Oceanic and Atmospheric Administration, as part of the Outer Continental Shelf Environmental Assessment Program.

We are grateful for the sea level data supplied to us by H. Mofjeld and J. Schumacher of NOAA PMEL, J. Oswald of International Technology, R. Mitchel, D. Bain, and S. Hamrick of State of Alaska, Department of Natural Resources. We are indebted to W. Stringer of Geophysical Institute, University of Alaska, for preparing charts of the ice distribution and discussing essential features of the ice motion in the Bering Sea and Norton Sound.

REFERENCES

- Albright, M., Geostrophic wind calculations for AIDJEX, in *Sea Ice Processes and Models*, edited by R. S. Pritchard, pp. 402–409, University of Washington Press, Seattle, 1980.
- Brower, W. A., Jr., H. W. Searby, J. L. Wise, H. F. Diaz, and A. S. Prechtel, Climatic atlas of the outer continental shelf waters and coastal regions of Alaska, 443 pp., Arctic Environ. Inform. and Data Center, Anchorage, Alas., 1977.
- Cacchione, D. A., and D. E. Drake, Sediment transport in Norton Sound, Alaska, *USGS Open File Rep. 79-1555*, 88 pp., 1979.
- Camerlengo, A. L., and J. J. O'Brien, Open boundary conditions in rotating fluids, *J. Comput. Phys.*, 35, 12–35, 1980.
- Coon, M. D., G. A. Maykut, R. S. Pritchard, D. A. Rothrock, and A. S. Thorndike, Modeling the pack ice as an elastic-plastic material, *AIDJEX Bull.*, 24, 1–105, 1974.
- Doronin, Y. P., On the method to calculate compactness and drift of ice (in Russian), *Tr. Arkt. Antarkt. Nauchno Issled. Inst.*, 291, 5–17, 1970.
- Fathauer, T. F., A forecast procedure for coastal floods in Alaska, *NOAA Tech. Memo. NWS AR-23*, 27 pp., Natl. Oceanic and Atmos. Admin., Anchorage, Alas., 1978.
- Hansen, W., Hydrodynamical methods applied to the oceanographical problems, *Proceedings of the Symposium on Mathematical-Hydrodynamical Methods in Physical Oceanography, Mitteilungen des Instituts für Meereskunde der Universität Hamburg*, 1, pp. 25–34, Hamburg, Federal Republic of Germany, 1962.
- Henry, R. F., Storm surges in the southern Beaufort Sea, Internal Report, 41 pp., Beaufort Sea Proj., Inst. of Ocean Sci., Patricia Bay, Sidney, B. C., Canada, 1974.
- Hibler, W. D., Modelling pack ice as a viscous-plastic continuum, *J. Phys. Oceanogr.*, 9, 815–846, 1979.
- Kowalik, Z., A study of the M_2 tide in the ice-covered Arctic Ocean, Modeling, identification, control, *Norw. Res. Bull.*, 2(4), 201–223, 1981.
- Kowalik, Z., Storm surges in the Beaufort and Chukchi Seas, *J. Geophys. Res.*, 89(C6), 10,570–10,578, 1984.
- Kowalik, Z., and W. Johnson, Numerical Modeling of Storm Surges in the Norton Sound, final report, 131 pp., Inst. of Mar. Sci., Univ. of Alas., Fairbanks, 1985.
- Kowalik, Z., and J. B. Matthews, The M_2 tide in the Beaufort and Chukchi Seas, *J. Phys. Oceanogr.*, 12(7), 743–746, 1982.
- Leavitt, E., Surface-based air stress measurements made during AIDJEX, in *Sea Ice Processes and Models*, edited by R. S. Pritchard, pp. 419–429, University of Washington Press, Seattle, 1980.
- Leendertse, J. J., and S. K. Liu, Modeling of tides and circulations of the Bering Sea, Environmental Assessment of the Alaska Continental Shelf, Annual report. of principal investigators, vol. 5, Transport, pp. 87–108, Natl. Oceanic and Atmos. Admin., 1981.
- Macklin, S. A., Wind drag coefficient over first-year sea ice in the Bering Sea, *J. Geophys. Res.*, 88(C5), 2845–2852, 1983.
- McNutt, L. S., Remote sensing analysis of ice growth and distribution in the eastern Bering Sea, in *The Eastern Bering Sea Shelf: Oceanography and Resources*, edited by D. W. Hood and A. Calder, pp. 141–165, University of Washington Press, Seattle, 1981.
- Mofjeld, H. O., Recent observations of tides and tidal currents from the northeastern Bering Sea shelf, *NOAA Tech. Memo. ERL PMEL-57*, 36 pp., Pac. Mar. Environ. Lab., Wash., 1984.
- Muench, R. D., and K. Ahlnäs, Ice movement and distribution in the Bering Sea from March to June 1974, *J. Geophys. Res.*, 81(24), 4467–4476, 1976.
- Muench, R. D., R. B. Tripp, and J. D. Cline, Circulation and hydrography of Norton Sound, in *The Eastern Bering Sea Shelf: Oceanography and Resources*, edited by D. W. Hood and A. Calder, pp. 77–93, University of Washington Press, Seattle, 1981.
- Overland, J. E., H. O. Mofjeld, and C. H. Pease, Wind-driven ice motion in a shallow sea, *J. Geophys. Res.*, 89(C4), 6525–6531, 1984.
- Pearson, C. A., H. O. Mofjeld, and R. B. Tripp, Tides of the eastern

- Bering Sea Shelf, in *The Eastern Bering Sea Shelf: Oceanography and Resources*, edited by D. W. Hood and A. Calder, pp. 111–130, University of Washington Press, Seattle, 1981.
- Pease, C. H., and J. E. Overland, An atmospherically driven sea-ice drift model for the Bering Sea, *Ann. Glaciol.*, 5, 111–114, 1984.
- Ray, V. M., and W. R. Dupré, The ice-dominated regimen of Norton Sound and adjacent areas of the Bering Sea, in *The Eastern Bering Sea Shelf: Oceanography and Resources*, edited by D. W. Hood and A. Calder, pp. 263–278, University of Washington Press, Seattle, 1981.
- Raymond, W. H., and H. L. Kuo, A radiation boundary condition for multidimensional flow, *Q. J. R. Meteorol. Soc.*, 110, 535–551, 1984.
- Reid, R. O., and B. R. Bodine, Numerical model for storm surges in Galveston Bay, *J. Waterw. Harbors Coastal Eng. Div. Am. Soc. Civ. Eng.*, 94(WWI), 33–57, 1968.
- Reynolds, M., and C. H. Pease, Drift characteristics of northeastern Bering Sea ice during 1982, *NOAA Tech. Memo. ERL PMEL-55*, 135 pp., Pac. Mar. Environ. Lab., Seattle, Wash., 1984.
- Roache, P. J., *Computational Fluid Dynamics*, 446 pp., Hermosa, Albuquerque, N. M., 1972.
- Sallenger, A. J., Jr., Measurements of debris-line elevations and beach profiles following a major storm: Northern Bering Sea coast of Alaska. *USGS Open File Rep. 83-394*, 1983.
- Schumacher, J. D., and R. B. Tripp, Response of northeast Bering Sea shelf waters to storms (abstract), *Eos Trans. AGU*, 60(46), 856, 1979.
- Stringer, W. J., and R. D. Henzler, Ice displacement vectors measured in Norton Sound and the adjacent Bering Sea, 1973–1979, report, 37 pp., Natl. Oceanic and Atmos. Admin., Outer Continental Shelf Environmental Assessment Project, 1981.
- Walter, B. A., and J. E. Overland, Air-ice drag coefficients for first-year sea ice derived from aircraft measurements, *J. Geophys. Res.*, 89(C3), 3550–3560, 1984.
- Wise, J. L., A. L. Comiskey and D. Becker, Jr., Storm surge climatology and forecasting in Alaska, 26 pp., Arctic Environ. Inform. and Data Center, Univ. of Alas., Anchorage, 1981.
-
- W. R. Johnson and Z. Kowalik, Institute of Marine Science, University of Alaska, Fairbanks, AK 99775.

(Received August 19, 1985;
accepted December 31, 1985.)